J Math Chem (2009) 45:417–430
DOI 10.1007/s10910-008-9415-2

ORIGINAL PAPER

Double toroids as model systems for carbon nanotube junctions: through-bond currents

E. Lijnen · A. Ceulemans · M. V. Diudea · Cs. L. Nagy

Published online: 1 August 2008

Abstract We show that the through-bond currents in a closed molecular network originate from their topologically invariant edge-homologies. When applied to double toroidal structures they give rise to topologically induced currents whose 3D manifestations are highly sensitive to the way both loops are merged together i.e. on the nature of their junction.

Keywords Carbon nanotube junctions · Through-bond currents · Topology · Homology

1 Introduction

Junctions of carbon nanotubes could form the basis of a whole new scala of nanostructures. In the present paper we study tetrapod junctions made of a negative curvature network joining four nanotubes. The open nanotube ends are pairwise connected into two loops forming a double toroid. Through-bond currents in this topology can be studied using the symmetry extensions of Eulers theorem [1].

Tight-binding band calculations for tetrapod junctions have recently been presented by Nakada et al. [2] and the geometry of carbon nanotube junctions has been described by László [3]. The starting point of our analysis is the celebrated polyhedral theorem, which relates the number of vertices (atoms), edges (bonds) and faces of a molecular network. For a polyhedron which can be mapped on a sphere one has:

E. Lijnen (✉) · A. Ceulemans
Departement Chemie, INPAC: Institute for Nanoscale Physics and Chemistry, K.U. Leuven, Celestijnenlaan 200F, 3001 Leuven, Belgium
e-mail: erwin.lijnen@chem.kuleuven.be

M. V. Diudea · Cs. L. Nagy
Faculty of Chemistry and Chemical Engineering, Babes-Bolyai University, 400084 Cluj, Romania

$$V - E + F = 2 \tag{1}$$

This formula was already known to Euler and dates back to the middle of the 18th century [4]. Extensions to networks on more intricate topologies and in higher dimensional spaces were subsequently made by Schläfli [5] and Poincaré [6]. In the present article we limit ourselves to molecular networks on 2D-closed surfaces for which the highest-dimensional components are faces. The Euler equation for networks on these surfaces reads:

$$V - E + F = 2 - 2g \tag{2}$$

where g stands for the genus or the number of 'holes' in the surface [7]. For example, a torus will be of genus 1 as it has one hole, whereas the double torus has two holes and therefore genus 2. Less well known is the adaptation of (2) to a more general form where instead of just numbers one relates the induced representations spanned by the different components of the polyhedron [1]:

$$\Gamma_\sigma(v) - \Gamma_\uparrow(e) + \Gamma_\odot(f) = \Gamma(H_0) - \Gamma(H_1) + \Gamma(H_2) \tag{3}$$

The terms on the right-hand side of (3) are of special interest as they correspond with the topological invariants or homologies of the polyhedron and can be used to derive the topologically induced through-bond currents of the polyhedron.

In Sect. 2 we give a brief introduction into the theory of polyhedral complexes which are the mathematical analogues of what a chemist would call a polyhedron. In Sect. 3 we discuss the basic concepts of homology theory which lie at the basis of the symmetry extension of the Euler equation, and explain the symmetry extended forms of the Euler equation (3). Finally in Sect. 4 we will make use of the firm mathematical foundations of the previous sections to investigate the topologically induced through-bond currents of some double-toroidal networks which may be envisaged as the junction of two carbon nanotube loops.

2 Polyhedral complexes

In the chemical literature a polyhedron refers to a molecular network (consisting of atoms and bonds) mapped on a 2D surface which encloses a finite region of space. Its constituting components are denoted as vertices, V, edges, E, and faces, F. Turning from chemistry to mathematics one must become acquainted with the ingredients of a polyhedral complex in the mathematical sense [8]. In principle a mathematical complex has the same ingredients as its chemical analogues but there are some non-trivial amendments.

The structural elements at the lowest level are trivial and correspond with zero-dimensional vertices, denoted as v^i. At the next level we find the one-dimensional edges which are no longer just lines connecting two vertices, but rather vector-like objects, pointing from one vertex to another. An edge can thus be represented as an ordered pair $(v^i v^j)$ where we agree to identify the first vertex v^i as the tail and the

second vertex v^j as the head of the vector. The ordering is of course purely a matter of choice but we can always say that the edges $(v^i v^j)$ and $(v^j v^i)$, with vertex order inverted, are related by the equation:

$$(v^i v^j) = -(v^j v^i) \tag{4}$$

At the third and highest level, we find the two-dimensional faces, which are nothing else than an ordered closed loop of vertices. For instance, a triangular face consisting of the vertices v^i, v^j, v^k, may be denoted as the ordered trio $(v^i v^j v^k)$ and forms a closed loop, $v^i \to v^j \to v^k \to v^i$. The ordering of the vertices provides the face with a rotor-like behavior. Again, if we invert the ordering, we invert the sense of rotation, and we can write:

$$(v^i v^j v^k) = -(v^k v^j v^i) \tag{5}$$

As in all organised structures consecutive layers are in contact. The top-down descent from higher to lower dimensional objects is called bordering or taking the boundary. The boundary of a face is the sum of the arrows along the surrounding edges, and can be most easily written in a simple pictorial way as:

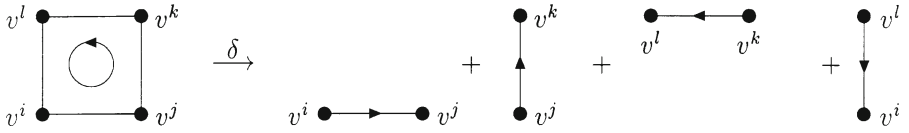

or as:

$$\delta(v^i v^j v^k) = (v^i v^j) + (v^j v^k) + (v^k v^l) + (v^l v^i) \tag{6}$$

where the Greek letter δ represents the boundary operation. Similarly the boundary of an edge is the difference between its head and its tail:

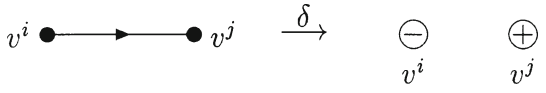

or:

$$\delta(v^i v^j) = v^j - v^i \tag{7}$$

Before we can turn to the interpretation of the symmetry extended Euler equation, we must first define the action of the point-group symmetries of a polyhedron on its constituting elements. For the vertices the action of a symmetry operation R is very simple as it just carries this vertex onto another vertex of the complex. Hence we can write:

$$Rv^i = v^{R_i} \tag{8}$$

where R_i is the image of vertex i under this mapping. All higher dimensional ingredients of the complex are built up from ordered combinations of vertices so (8) will be sufficient to define the action of a symmetry element R on all components. Indeed for an ordered pair one has:

$$R(v^i v^j) = (v^{R_i} v^{R_j}) \tag{9}$$

where the resulting image is once again an edge of the complex, although it might be that it was defined in the opposite sense as $(v^{R_j} v^{R_i})$ in which case we can always write

$$R(v^i v^j) = -(v^{R_j} v^{R_i}) \tag{10}$$

Finally the same can be said for the faces, where the image must once again be a face of the polyhedron although its sense of rotation could be opposite to the sense originally defined for the face.

We are now fully equipped to determine the transformation matrices which describe the action of the symmetry elements on the different components of the polyhedral complex. In general these representations will be reducible but they can always be decomposed into irreducible representations using the standard techniques of character theory [9]. The resulting sets of irreps are denoted as $\Gamma_\sigma(v)$, $\Gamma_\uparrow(e)$ and $\Gamma_\odot(f)$ for respectively the vertices, the edges and the faces where the indices $\sigma, \uparrow, \odot$ refer to the scalar, vector and rotor-like behavior of these different layers of organisation. The symmetry extended Euler equation is now just a restatement of the original Euler equation where the numbers of components are replaced by their corresponding irreps under the symmetry group of the complex. For a simple spherical complex one then has:

$$\Gamma_\sigma(v) - \Gamma_\uparrow(e) + \Gamma_\odot(f) = \Gamma_0 + \Gamma_\epsilon \tag{11}$$

This equation shows us that if we take the alternating sum over the irreps of the different structural components we end up with two one-dimensional irreps Γ_0 and Γ_ϵ. They are readily distinguished from the other irreps as they are the only ones which do not find a counterpart within the set of irreps on the edges and therefore survive taking the alternating sum.

As an easy example to (11), in Fig. 1 we give a pictorial scheme of the different irreps for a tetrahedral complex of T_d symmetry. Substituting these irreps into (11) gives:

$$\Gamma_\sigma(v) - \Gamma_\uparrow(e) + \Gamma_\odot(f) = A_1 + T_2 - T_2 - T_1 + A_2 + T_1 = A_1 + A_2 \tag{12}$$

The two surviving irreps can be identified as the vertex representation A_1 and the face representation A_2 and are the only elements which are not the boundary of a higher dimensional component or which have no lower dimensional boundary. They form a set of topological invariants of the complex and within mathematics they are called homologies.

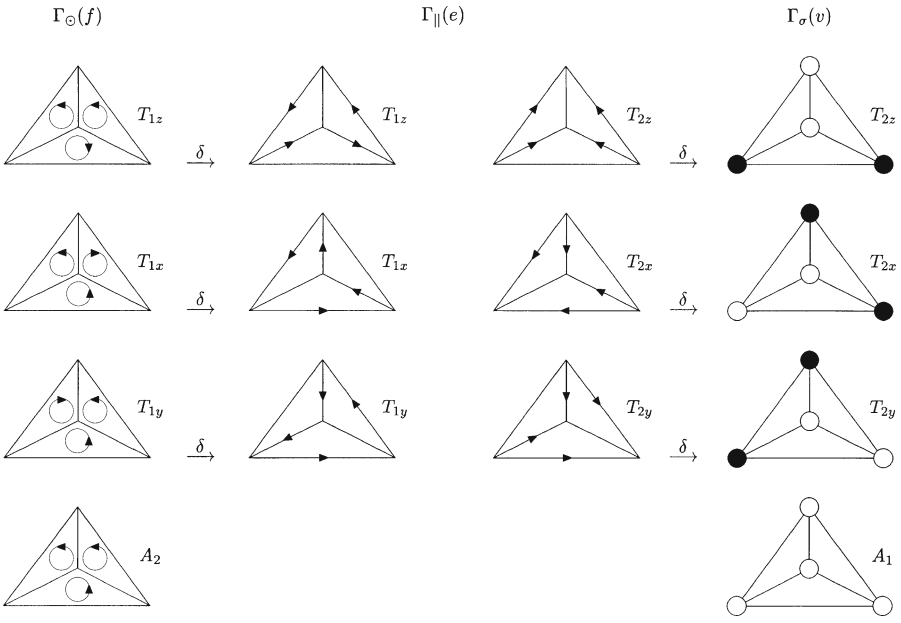

Fig. 1 Symmetry adapted linear combinations for the different components of a tetrahedral complex

The first homology for the sphere corresponds with a vertex homology Γ_0 transforming as the totally symmetrical representation (A_1 within T_d). It can be seen as resulting from an electric monopole in the center of the complex which results in equal charges on all vertices of the network and hence no net current flow over the edges. The second spherical homology is a face homology Γ_ϵ transforming as the pseudo-scalar representation (A_2 within T_d). Its easiest interpretation comes from considering a magnetic monopole located in the center of the complex and leading to a set of equally-sensed face rotors. For this special face-representation the projection of the face-rotors onto the edges leads to equally large but opposing current-flows on all edges which nicely cancel out. In other words, there is no edge-boundary for this face-representation. These two homologies are however not solely restricted to the sphere, but show up in all 2D oriented complexes of higher genera. In (2) they can be related to the "2" directly following the equation sign. The other term "$-2g$" is, as we shall see in the next section, completely due to edge-homologies. For the sphere, $g = 0$, such edge-homologies are obviously absent, but turning to higher topologies, the addition of every new hole in the surface, $g+=1$, creates two extra edge-homologies. These edge-homologies play a central role in the remainder of this article as they lie at the basis of the topologically invariant through-bond currents.

3 Homology groups

In order to find the homologies of a given complex we start from the definition of a p-chain [10,11]:

A p-chain c_p in a complex is a linear combination of p-dimensional objects with integer coefficients

$$c_p = \sum_i \kappa_i (v^{i_1}, \ldots, v^{i_{p+1}}) \tag{13}$$

Two p-chains of the same dimension can be added by adding their coefficients. In this way the p-chains generate a group, the p-chain group C_p, which is isomorphic to direct sums of $\mathbf{Z}$. A general theorem of homology theory states that—in the absence of torsion—this p-chain group C_p can be further factorized as:

$$\begin{aligned} C_p &\cong Z_p \oplus B_{p-1} \text{ with} \\ Z_p &= ker\, \delta_p \\ B_p &= im\, \delta_{p+1} \end{aligned} \tag{14}$$

The p-cycle group, Z_p, is the kernel of the boundary operation δ_p and thus contains all elements of C_p that have no boundary in the chains with one dimension less. The p-boundary group, B_p, is the image of the boundary operation δ_{p+1} and therefore collects all the elements of C_p that are themselves boundaries of chains with one dimension more. Note that B_p is always a subgroup of Z_p as $\delta_p \delta_{p+1} = \emptyset$. We can thus form the quotient group:

$$H_p = Z_p / B_p \tag{15}$$

where H_p is called the p-th homology group. The homology groups thus measure the extent to which the complex has p-cycles which are not boundaries. Using (15) we can factorize the p-chain group even further:

$$C_p \cong H_p \oplus B_p \oplus B_{p-1} \tag{16}$$

A detailed description how these homology groups can be calculated will be deferred to a separate publication. Here we restrict ourselves to the listing (Table 1) of the different groups connected to the tetrahedral complex. The cycle-groups C_0, C_1 and C_2 are listed at the top of the table and are resp. isomorphic to $\mathbf{Z}^V$, $\mathbf{Z}^E$ and $\mathbf{Z}^F$. Beneath them one also finds their complete decomposition in terms of (16). When we now, like in the original Euler equation, take the alternating sum over the cycle-groups we obtain:

$$C_0 - C_1 + C_2 = H_0 + B_0 - B_0 - B_1 + H_2 + B_1 = H_0 + H_2 \tag{17}$$

This exactly parallels the result of (11) where however irreducible representations are assigned to homology groups. This assignment provides interesting additional information to the homology groups, allowing to discriminate homology groups with the same p, as will be discussed in the next section. A thorough account of the connection between both Eqs. 17 and 12, namely between the homology groups of oriented

Table 1 Groups of the tetrahedral complex and their corresponding irreducible representations

$C_0 \cong \mathbf{Z}^4$	$C_1 \cong \mathbf{Z}^6$	$C_2 \cong \mathbf{Z}^4$
$H_0 \cong \mathbf{Z}^1 \to A_1$	$H_1 \cong \mathbf{Z}^0 \to \emptyset$	$H_2 \cong \mathbf{Z}^1 \to A_2$
$B_{-1} \cong \mathbf{Z}^0 \to \emptyset$	$B_0 \cong \mathbf{Z}^3 \to T_2$	$B_1 \cong \mathbf{Z}^3 \to T_1$
$B_0 \cong \mathbf{Z}^3 \to T_2$	$B_1 \cong \mathbf{Z}^3 \to T_1$	$B_2 \cong \mathbf{Z}^0 \to \emptyset$

complexes and the irreducible symmetries of their corresponding symmetry groups, can be found in Ref. [12]. The connection between both descriptions is also indicated in Table 1.

4 Currents on double toroids

Before we turn to the discussion of the edge-currents on double-toroidal networks, we first review some results for the torus for which the extended Euler equation reads[13]:

$$\Gamma_\sigma(v) - \Gamma_\uparrow(e) + \Gamma_\odot(f) = \Gamma_0 + \Gamma_\epsilon - \Gamma_{R_z} - \Gamma_{T_z} \tag{18}$$

As indicated before the representations Γ_0 and Γ_ϵ correspond to the ubiquitous vertex and face homologies. The other terms represent the two edge-homologies and are drawn schematically in Fig. 2. The first of them, Γ_{R_z}, corresponds with a charge flow along the loop of the torus and transforms in exactly the same way as a magnetic dipole. The second one, Γ_{T_z}, gives rise to a whirling motion around the spine of the torus. It has the symmetry of an electric dipole and can be seen to result from an *anapole* moment i.e. a circular magnetic field inside the torus. An interesting situation occurs when the torus is decorated with a chiral network, as in this case both moments can interact, giving rise to helical charge flows [14]. This clearly indicates that networks on higher-genus surfaces can sustain interesting non-trivial edge-currents which are inaccessible for simple spherical networks.

The next surface, after the sphere and the torus, is the double torus or 'pretzel', which can be formed by connecting two toroidal loops to a common junction with four pore holes. Various types of junctions can be constructed where the geometry and symmetry of the junction will have a direct effect on the spatial realisations of the resulting edge-current patterns. For our current examples, we limit ourselves to trivalent networks which obey the following formula:

$$\sum_n (n-6) f_n = 12(g-1) \tag{19}$$

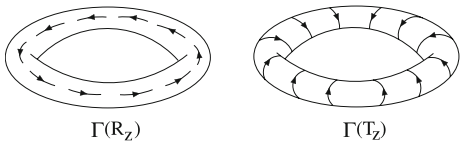

Fig. 2 Schematical representation of the two edge-homologies of a torus

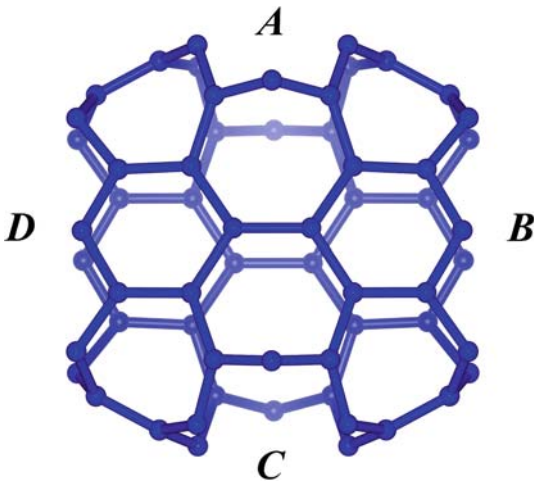

Fig. 3 Trivalent junction with 12 heptagonal defects exhibiting D_{2h} symmetry

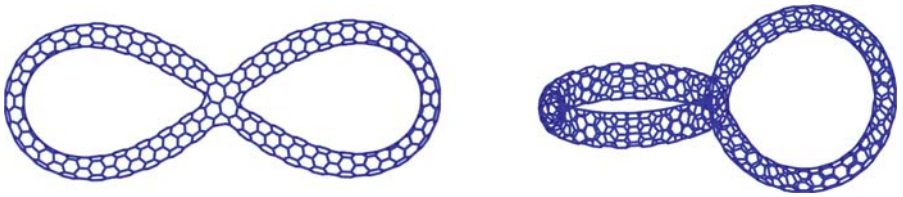

Fig. 4 Flat (Left) and staggered (Right) double torus build from the junction shown in Fig. 3

The summation runs over all possible face sizes n with f_n indicating the number of faces of size n. For a double torus, $g = 2$, the RH-side of (19) reads "12", which can be accomplished by starting with a hexagonal lattice and adding some heptagonal, octagonal or even nonagonal defects. The only restriction is that the total weight of the defects should equal "12", so one can for instance take 12 heptagons ($12 \times (7-6) = 12$), 6 octagons ($6 \times (8-6) = 12$), 4 nonagons, ($4 \times (9-6) = 12$), or a well-chosen combination thereof.

The first two examples of double toroidal networks we will investigate are both constructed from the junction shown in Fig. 3. It has 12 heptagonal defects and as a stand-alone entity it exhibits D_{2h} spatial symmetry. To form a double torus out of this junction one has to make pairwise connections between the four holes, labeled A to D in Fig. 3, which can be done in essentially two different ways. A first way consists in the pairwise linkage of neigboring holes ($A \rightarrow B$ and $C \rightarrow D$). These connections can be easily made by loops which lie in the same plane as the junction, thereby leading to a "flat" double torus. In a second way, oppositely lying holes ($A \rightarrow C$ and $B \rightarrow D$) are identified. In this case both connecting loops are obligated to leave the plane leading to a "twisted" double torus. The connections between the holes can always be performed by an all-hexagon carbon nanotube for which the diameter exactly matches the diameter of the holes. In Fig. 4 we show both a flat and a staggered double torus based on the junction of Fig. 3.

Table 2 Characters of the vertices, edges and faces for the flat double torus under the symmetry elements of C_{2h}

	E	C_2	i	σ_h
V	60	0	0	8
E	90	−2	0	4
F	28	0	0	−4

From a topological point of view, the lengths of the connecting nanotubes are however immaterial as they do not change the overall topology of the resulting structure. In the following, we will therefore link the holes by a single ring of hexagons. This has the main advantage that, while still fully grasping the topological implications of the junction, it reduces the number of ingredients of the complex (V, E, F) to an absolute minimum, thereby greatly simplifying the calculations of the edge-homologies.

Let us start with the "flat" double torus build from the junction of Fig. 3. Although the stand-alone junction has D_{2h} symmetry, the attachment of both loops leads to a closed structure with only C_{2h} symmetry. The characters for the vertices, edges, and faces under the four operations of this group can be found in Table 2. A reduction of these representations into irreps leads to:

$$\begin{aligned}\Gamma_\sigma(v) &= 17A_g + 13B_g + 13A_u + 17B_u \\ \Gamma_\uparrow(e) &= 23A_g + 22B_g + 21A_u + 24B_u \\ \Gamma_\odot(f) &= 6A_g + 8B_g + 8A_u + 6B_u\end{aligned} \tag{20}$$

Comparing these results with the general expression of the symmetry extended Euler equation:

$$\Gamma_\sigma(v) - \Gamma_\uparrow(e) + \Gamma_\odot(f) = \Gamma(H_0) - \Gamma(H_1) + \Gamma(H_2) \tag{21}$$

we find the following homologies:

$$\begin{aligned}\Gamma(H_0) &= A_g \\ \Gamma(H_1) &= A_g + A_u + B_g + B_u \\ \Gamma(H_2) &= A_u\end{aligned} \tag{22}$$

Note that simply taking the alternating sum in this case would lead us to the false result that there are only two homologies namely the edge-homologies transforming as B_g and B_u. If we however take into account that there must always exist one vertex-homology transforming as the total symmetric representation and one face-homology transforming as the pseudoscalar representation, we will end up with the correct result of (22). In Fig. 5 we show the A_g edge-homology, with the exact directions and magnitudes of the flows indicated for each edge. We however limited ourselves to the upper part of the network as the flows on the lower part can be easily reconstructed by use of the A_g symmetry. A visual inspection shows that this special edge-representation indeed corresponds with an edge-homology. It has no vertex-boundary because at every vertex the sum of the incoming and outgoing currents is nicely balanced, leading to

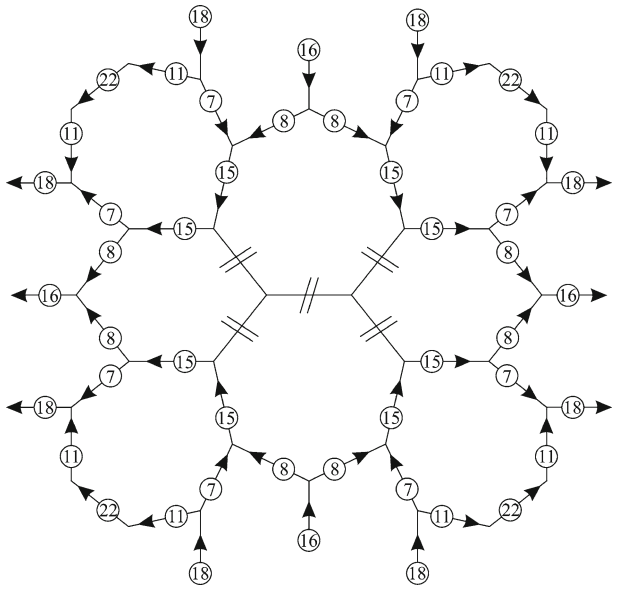

Fig. 5 A_g edge-homology for a flat double torus build from the junction of Fig. 3

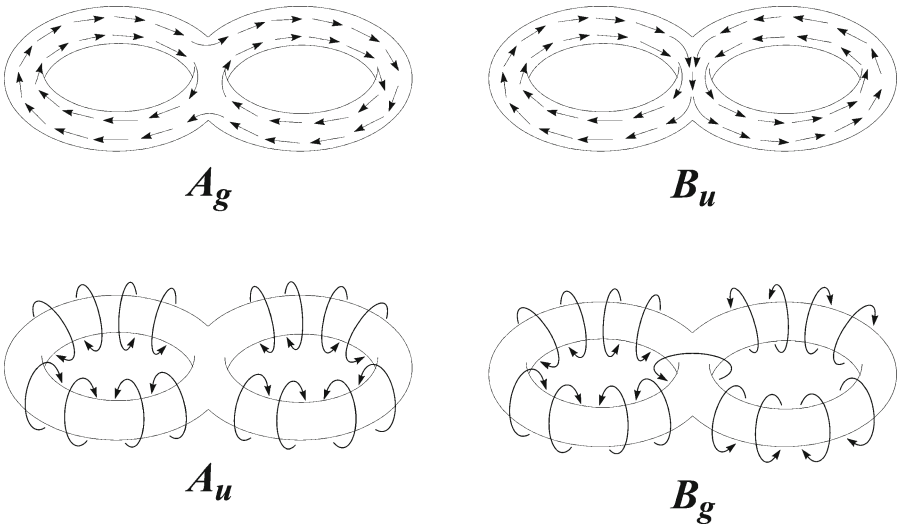

Fig. 6 Current-flows corresponding with the four edge-homologies of the flat double torus

no net buildup of charges on the vertices. At the same time, for every face, the sums of the left and right turning currents are equal. There is thus no net current-rotation on any of the faces, meaning that this A_g edge-representation does not form the boundary of some higher face-representation. As we saw earlier, these are exactly the two conditions for being an edge-homology. It would be quite tedious to visualize all the homologies in such a detailed form. We rather limit ourselves to a more schematical

Table 3 Characters of the vertices, edges and faces for the staggered double torus under the symmetry elements of C_{2v}

	E	C_2	$\sigma_v(xz)$	$\sigma_v(yz)$
V	60	0	8	4
E	90	−6	−2	−6
F	28	0	−10	−10

approach but which still reveals the main features of the edge-flows. In Fig. 6 one can find such schemes for the four edge-homologies of our flat double torus. The A_g homology shows conrotating current flows around the loops which mostly cancel each other out at centre of the junction as could be seen from Fig. 5. The B_u homology on the contrary consists of counter rotating current flows on both loops, which by their cooperative effect lead to significant currents through the junction. Both other homologies give rise to anapole moments resulting from whirlings around the loops. In the A_u case both whirlings are conrotating and thereby once again deplete the edge-currents on the junctions center, whereas the B_g representation leads to counter rotating anapoles reinforcing the currents on the junctions center while even creating a whirling motion around the junction itself. These four edge-homologies give rise to nice topological invariant edge-currents which are clearly separated by symmetry. On the other hand they are fairly straightforward summations or subtractions of the single torus invariants, as symmetry dictates.

The case where opposite holes of the junction of Fig. 3 are connected will however show some more intricate behaviour. Due to its staggered form, its spatial symmetry is limited to C_{2v}. The characters of the different components under this symmetry are given in Table 3, and reduce to the following irreps:

$$\begin{aligned}\Gamma_\sigma(v) &= 18A_1 + 12A_2 + 16B_1 + 14B_2\\ \Gamma_\uparrow(e) &= 19A_1 + 23A_2 + 25B_1 + 23B_2\\ \Gamma_\odot(f) &= 2A_1 + 12A_2 + 7B_1 + 7B_2\end{aligned} \tag{23}$$

giving rise to the following homologies:

$$\begin{aligned}\Gamma(H_0) &= A_1\\ \Gamma(H_1) &= 2B_1 + 2B_2\\ \Gamma(H_2) &= A_2\end{aligned} \tag{24}$$

Inspection of (24) shows that the spatial symmetry group C_{2v} does no longer allow us to fully distinguish the four edge-homologies by their representational signature. Fortunately this problem can be circumvented, if instead of its spatial symmetry one makes use of the full combinatorial symmetry group of the complex. Recall that the combinatorial symmetry group of a complex is defined as all vertex-permutations which map vertices onto vertices, edges onto edges and faces onto faces. For the present case, the combinatorial symmetry group of the complex is isomorphic to D_{2h},

Table 4 Characters of the vertices, edges and faces for the staggered double torus under the symmetry elements of D_{2h}

	E	$C_2(z)$	$C_2(y)$	$C_2(x)$	i	σ_{xy}	σ_{xz}	$\sigma_{(yz)}$
V	60	0	0	0	0	8	8	0
E	90	−6	0	0	0	4	−2	−6
F	28	0	2	2	0	−4	−10	−10

which corresponds exactly with the symmetry of the stand-alone junction. Indeed, as a purely combinatorial object, the double toroidal network does not need to worry about self-intersections thereby lifting the symmetry-breaking restriction that the connecting loops should leave the plane of the junction. In Table 4 we present the characters under this full combinatorial D_{2h} producing the following sets of irreps:

$$\begin{aligned}
\Gamma_\sigma(v) &= 10A_g + 5A_u + 7B_{1g} + 7B_{2g} + 6B_{3g} + 8B_{1u} + 8B_{2u} + 9B_{3u} \\
\Gamma_\uparrow(e) &= 10A_g + 11A_u + 12B_{1g} + 12B_{2g} + 11B_{3g} + 9B_{1u} + 12B_{2u} + 13B_{3u} \\
\Gamma_\odot(f) &= A_g + 7A_u + 5B_{1g} + 4B_{2g} + 4B_{3g} + B_{1u} + 3B_{2u} + 3B_{3u}
\end{aligned} \tag{25}$$

which provides a full symmetry resolution of the four edge-homologies:

$$\begin{aligned}
\Gamma(H_0) &= A_g \\
\Gamma(H_1) &= B_{2g} + B_{3g} + B_{2u} + B_{3u} \\
\Gamma(H_2) &= A_u
\end{aligned} \tag{26}$$

Schematic sketches of the edge-homologies are given in Fig. 7. The B_{2u} and B_{3u} modes are easy to interpret. They both correspond to a current flow around one of the loops together with the total absence of any edge current within the other loop. So contrary to the flat double torus, the symmetry of the present system forbids a coupling between circular edge-currents on both staggered loops. The remaining two invariants, B_{2g} and B_{3g}, form very special cases as they couple an anapole-like moment in one of their loops to a strange looking edge-current in the second loop consisting of two oppositely running circular currents at the inside and the outside of the loop. A physical interpretation of such a current is not straightforward but similar counter-rotating currents have been predicted within a benzene molecule as a non-linear response to high external homogeneous magnetic fields [15].

As a last example we will study the double-toroidal network based on the tetrapod junction of Fig. 8. It is built from four nonagonal defects and exhibits T_d symmetry which will however be lowered to D_{2d} symmetry by the addition of two loops. Using the corresponding characters of Table 5 we can easily derive the irreps:

$$\begin{aligned}
\Gamma_\sigma(v) &= 4A_1 + 2A_2 + 2B_1 + 2B_2 + 6E \\
\Gamma_\uparrow(e) &= 3A_1 + 5A_2 + 4B_1 + 4B_2 + 10E \\
\Gamma_\odot(f) &= 3A_2 + 3B_1 + 2E
\end{aligned} \tag{27}$$

which translate in the following homologies:

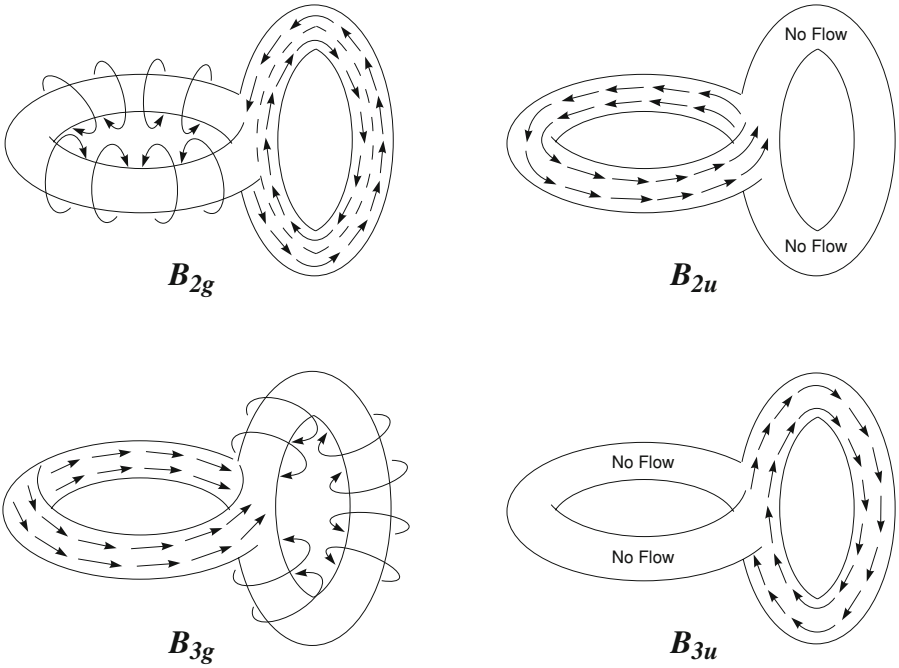

Fig. 7 Current-flows corresponding with the four edge-homologies of the staggered double torus

Fig. 8 Trivalent junction with four nonagonal defects exhibiting D_{2d} symmetry

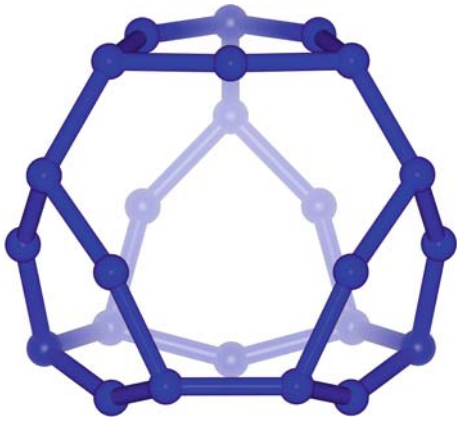

$$\begin{aligned}\Gamma(H_0) &= A_1\\ \Gamma(H_1) &= 2E\\ \Gamma(H_2) &= B_1\end{aligned} \tag{28}$$

The edge-homologies can be seen to transform as two double degenerated E representations. A complete separation based on the spatial symmetry group of the complex is therefore impossible. The combinatorial symmetry group of the complex will

Table 5 Characters of the vertices, edges and faces for the staggered double torus under the symmetry elements of D_{2d}

	E	$2S_4$	C_2	$2C_2'$	$2\sigma_d$
V	24	0	0	0	4
E	36	0	−4	−2	−2
F	10	0	2	0	−6

not cure this problem as it is isomorphic with the spatial group. Apparently in this case the edge-homologies are degenerate and dipolar and anapolar modes can mix freely.

5 Conclusions

The double torus or 'Pretzel' corresponds to two toroidal loops that are connected to a common junction with four pore holes. Various types of junctions can be constructed. We have studied three examples of symmetric junctions, based on trivalent graphs, consisting of a hexagonal lattice with heptagonal and nonagonal defects, representing a flat, staggered and tetrapod type junction of four carbon nanotubes. For all these double tori bond-currents were constructed that correspond to topological invariant edge-homologies and represent the principal electric and magnetic moments of the molecular frame. For two cases the spatial or combinatorial symmetry of the junction leads to a complete resolution of the edge-homologies while for the tetrahedral tetrapod junction the edge-homologies follow identical representations and can be combined freely. Most interestingly in the case of the staggered geometry with heptagonal defects an anapole moment on one ring is coupled through the junction to a combination of circular currents on the other ring. As these examples show, a variety of patterns is to be expected for the transmission of bond currents through carbon nanotube junctions.

Acknowledgements E. Lijnen holds a post-doctoral fellowship from the Fund for Scientific Research—Flanders.

References

1. A. Ceulemans, P.W. Fowler, Nature (London) **353**, 52–54 (1991)
2. K. Nakada, K. Maeda, K. Daigoku, J. Math. Chem. (submitted)
3. I. László, Croat. Chem. Acta **78**, 217–221 (2005)
4. L. Euler, Elementa Doctrinae Solidorum, Opera Omnia, Ser. 1, **26**(XIV–XVI), 71 (1752)
5. L. Schläfli, *Theorie der vielfachen Kontinuität, Neue Denkschriften der allgemeinen schweizerischen Gesellschaft für die gesamten Naturwissenschaften* Band 38, IV (Zürich) (1901)
6. H. Poincaré, Compt. Rend. (Paris) **117**, 144 (1893)
7. J.L. Gross, T.W. Tucker, *Topological Graph Theory* (Dover Publ. Inc., New York, 2001)
8. A. Ceulemans, E. Lijnen, Eur. J. Inorg. Chem. **7**, 1571–1581 (2002)
9. F.A. Cotton, *Chemical Applications of Group Theory*, 3rd edn. (Wiley, New York, 1990)
10. P.J. Hilton, S. Wylie, *Homology Theory* (Cambridge University Press, Cambridge, 1960)
11. P.J. Giblin, *Graphs, Surfaces and Homology* (Chapman and Hall, London, 1977)
12. A. Ceulemans, M. Szopa, P.W. Fowler, Eur. Phys. Lett. **36**, 645–649 (1996)
13. A. Ceulemans, P.W. Fowler, J. Chem. Soc. Faraday Trans. **91**, 3089–3093 (1995)
14. A. Ceulemans, L.F. Chibotaru, P.W. Fowler, Phys. Rev. Lett. **80**, 1861–1864 (1998)
15. A. Soncini, P.W. Fowler, Chem. Phys. Lett. **400**, 213–220 (2004)